UNDAMPED PASSIVE ATTITUDE STABILIZATION AND ORBIT MANAGEMENT OF A 3U CUBESAT WITH DRAG SAILS

Siddharth S. Kedare[*] and Steve Ulrich[†]

This paper evaluates the effectiveness of drag sails on maintaining a ram-facing orientation for a 3U CubeSat in Equatorial Low Earth Orbit. The influence of varying the drag sail area and inertia tensor on the aerostabilization characteristics and orbit of the spacecraft is examined through computational modeling of the spacecraft dynamics in Matlab-Simulink. The study also investigates the ability of a commercially available attitude control system to slew the spacecraft into a low-drag orientation to extend orbital lifetime. The results indicate that undamped aerostabilization of a 3U CubeSat is feasible, and provides acceptable conditions for limited scientific observation. In addition, the simulation results demonstrate that the spacecraft is capable of entering and maintaining a low-drag orientation for five days without reaction wheel saturation.

INTRODUCTION

CubeSats are part of a niche satellite market emerging from the desire of the academic and scientific community to perform rapidly developed, cost-effective missions using very small spacecraft. Having a cross-sectional profile of 10 cm × 10 cm, measuring between 10 and 30 cm in length, and a mass between 1 and 4 kilograms, CubeSats form a standardized platform for building satellites.[1] First developed in the late 1990s at California Polytechnic State University and Stanford University, the CubeSat was originally intended for educating students about the capabilities of Sputnik, the first man-made satellite put into orbit around the Earth. CubeSats provide a low-cost capability for university students and the academic community to develop and test scientific and space technology payloads. In September 2013, the Colorado Student Space Weather Experiment (CSSWE) 3U CubeSat, designed and built by students at the University of Colorado in Boulder, CO, was launched into space on an Atlas V rocket[*]. Funded by the National Science Foundation, the mission focused on investigating space weather through use of an energetic particle telescope. CubeSat platforms have also allowed developing nations to have access to space for scientific purposes. In May 2013, the Ecuadorian NEE-01 Pegaso technology demonstration satellite was launch on a Long March 2D rocket.[2] The mission focused on evaluating various thermal management technologies. In addition it demonstrated the successful in-flight implementation of ultra-thin deployable solar panels on a CubeSat platform.[3]

---

[*]M.A.Sc Candidate | now Research Affiliate, Department of Mechanical and Aerospace Engineering, Carleton University, 1125 Colonel By Drive, Ottawa ON K1S 5B6, Canada.

[†]Assistant Professor, Department of Mechanical and Aerospace Engineering, Carleton University, 1125 Colonel By Drive, Ottawa ON K1S 5B6, Canada.

[*]Colorado Student Space Weather Experiment, University of Colorado, 2014 (accessed June 1, 2014), http://lasp.colorado.edu/home/csswe

The use of the space environment for spacecraft control has been demonstrated in flight, though it has been limited to orbital management. The NanoSail-D2 3U CubeSat, deployed in January 2011, was built by NASA's Marshall Space Flight Center and Ames Research Center to study the deployment and effectiveness of solar sails on orbit[*]. Certain science operations such as Earth-horizon detection and atmospheric density mapping require the spacecraft to be aligned with the ram-facing direction. Such an orientation may also provides a 'safe-mode' in which communication capability can be maintained at all times with the satellite, without the control system actuators having to provide additional torque.

Along with the potential for low-cost mission with high scientific return, there are significant advantages in launching multiple CubeSats to perform missions typically assigned to larger satellites. In addition to cost savings and built-in redundancy, CubeSats offer mission flexibility and adaptability. However, the international satellite community is faced with the growing problem of orbital debris and space collision avoidance. In September 2007, the Inter-Agency Space Debris Coordination Committee (IADC) recommended that satellites deorbit within 25 years of mission completion, or 30 years of launch if the spacecraft is incapable of being maneuvered into a graveyard orbit.[4,5]

Previous Research

Early research on the effects of the atmosphere on the rotational dynamics of a spacecraft dates back to the late 1950s and early 1960s.[6,7] These studies concluded that passive aerodynamic stability was achievable at around 300 miles altitude and below, and that aerodynamic stabilization resulted in oscillatory behavior. The first on-orbit demonstration of aerostabilization of satellites was performed by the Soviet Union in 1967 (Cosmos 149) and 1970 (Cosmos (320).[8] These spacecraft utilized extended aerodynamic skirt stabilizers, and were nicknamed "space arrows". In 1996, the United States flight tested the PAMS on STS-77, demonstrating the feasibility of magnetically damped aerostabilization.[9–11] The PAMS experiment relied on offsetting the center of mass to one end of the satellite to achieve an aerodynamically stable configuration. Such an offset, however, is not allowed by the CubeSat Standard[†], and it was apparent that further research would be necessary to demonstrate the feasibility of aerostabilization for CubeSats.

Studies conducted at the University of Kentucky Space Systems Laboratory investigated the conditions required for stability of a 3U CubeSat with deployable side panels.[12] In 2010, the QbX spacecraft pair, developed by the US Naval Research Laboratory, successfully demonstrated the feasibility of aerodynamic stabilization and passive velocity-vector pointing for a 3U CubeSat at an altitude of 300km[13‡]. However, the QbX satellites required a complex damping system utilizing active actuators. To date, there have been no flight demonstrations of completely passive solutions for CubeSat stability.

Building on this research, in 2012, Rawashdeh and Lumpp[14] presented a completely passive solution for 3U and 1U CubeSat stabilization. Their study focused on the use of two aerodynamically stable designs - one based on the Pumpkin Colony-1 bus by Pumpkin Inc. and the other incorporating flexible spring steel drag fins in a 1U CubeSat bus. Both solutions utilized magnetic methods

---

[*]NASA's First Solar Sail NanoSail-D Deploys in Low-Earth Orbit, NASA, 2011 (accessed May 14, 2014), http://www.nasa.gov/mission_pages/smallsats/11-010.html

[†]CubeSat Design Specifications, The CubeSat Project - Cal Poly San Luis Obispo, 2014 (accessed Aug. 21, 2014), http://cubesat.org/index.php/documents/developers

[‡]NRL Launches Nanosatellite Experimental Platforms, Naval Research Laboratory, 2010 (accessed Aug. 23, 2014), http://www.nrl.navy.mil/media/news-releases/2010/nrl-launches-nanosatellite-experimental-platforms

for oscillation damping.

Significant research has been conducted towards the development of rapid deorbit technology for the CubeSat form factor. The CanX-7 satellite, funded by DRDC-Ottawa, NSERC, and COM DEV Ltd., is currently under development at the University of Toronto's Space Flight Laboratory. The mission, expected to launch in late 2014, aims to deploy a 5 m^2 lightweight, modular sail capable of meeting the deorbit requirements set by the IADC.[15] DeOrbitSail, a similar mission headed by Surrey Space Center and also slated to launch in 2014,[16] proposes the use of four triangular drag sails with a combined area of 25 m^2.

Contributions

In this context, the main contribution of this paper is the evaluation of the effect of varying the area of a CubeSat drag sail on the velocity-pointing (ram-facing) accuracy over seven days without the use of an active control system or magnetic hysteresis material for oscillation damping. Though previous research has established the oscillatory nature of aerostabilization[6,7] and examined its effectiveness with damping,[14] to our knowledge a quantitative study on the undamped stability characteristics for CubeSats has not been conducted. Four sail configurations are considered, consisting of drag sail pairs with areas of 5 m^2, 1 m^2 and 0.1 m^2, alongside a control configuration with no drag sails. The effect of these drag sail on the spacecraft orbit will also be examined for the duration of the simulation.

In addition, the effect of scaling the satellite inertia tensor on the oscillation frequency about the ram-facing direction will be evaluated. Such an inertia scaling would simulate the deployment of gravity gradient stabilization booms or scientific equipment. The original inertia tensor, **J**, is scaled by factors of 0.5, 2.0 and 4.0 for a 3U CubeSat configured with a pair of 5 m^2 drag sails. Examining the ability of the drag sails to maintain the CubeSat in a ram-pointing orientation for a variety of inertia tensors will aid in evaluating the flexibility of such a stabilization technique.

Lastly, the paper examines the ability of an active attitude control system (ACS) with limited torque and angular momentum capability to reorient the satellite from passive drag sail stabilization mode into a low drag configuration. The ACS must be capable of holding the satellite in such an orientation for a period of five days, and demonstrate a significant reduction in orbit decay compared to the passive stabilization mode. The selected maneuver is an eigenaxis rotation to an attitude state of $[90° \ 10° \ 0°]_{RPY}$ from passive stability mode.

SPACECRAFT DYNAMICS

Prior to the creation of the simulation environment, it was critical to establish the dominant forces and torques experienced by a satellite at the expected altitude of 600 km. As presented by Montenbruck and Gill,[17] in Low Earth Orbit (LEO), atmospheric drag and Earth oblateness are the dominant factors perturbing the orbit of a spacecraft. Furthermore, from Schrello[6] and GN&C criteria specified by NASA,[18] aerodynamic and gravity gradient torques are the dominant perturbations for the orbit under consideration. Based on this information, the scope of modeling the space environment was significantly reduced. Further details regarding these mathematical models shall be presented in this section.

Orbit Propagation Model

The rate of change of the orbital state vector can be defined as

$$\begin{bmatrix} \dot{\vec{r}} \\ \ddot{\vec{r}} \end{bmatrix} = \begin{bmatrix} \vec{v} \\ \ddot{\vec{r}}_{grav} + \ddot{\vec{r}}_{aero} \end{bmatrix} \tag{1}$$

where $\ddot{\vec{r}}_{grav}$ and $\ddot{\vec{r}}_{aero}$ are the forces due to gravity and aerodynamic drag respectively. Given an initial position, $\vec{r}_0$, and velocity, $\vec{v}_0$, the orbit propagator predicts the position and velocity of the spacecraft at each time step by integrating the orbital state change vector of the satellite.

Gravity Model Though multiple Earth gravity models exist, they can be all be broadly categorized into the simple spherical model and spherical harmonic models. The first assumes that the Earth is perfectly spherical, allowing the gravitational acceleration to be measured solely as a function of the distance from the center of the Earth. The spherical Earth assumption provides a good first approximation for the orbit of a spacecraft. However, it does does account for the oblate spheroid shape of the Earth, or the uneven distribution of mass within the Earth's lithosphere. The addition of the J_2 term, which accounts for the flattening of the Earth's poles due to its rotation, significantly improves the accuracy of the gravity model.

The inclusion of the J_2 term does not typically allow for precision orbit determination and propagation, as it neglects higher order gravitational terms. This brings about the need for elliptical and spherical harmonic gravitational models. Early examples of these models were the Goddard Earth Models developed at the Goddard Space Flight Center.[19] Modern implementations, derived from data collected by satellites, include the EGM-2008 (Earth Gravity Model) based on WGS-84 (World Geodetic System).[20] For the purposes of this study, a $J_{6,6}$ spherical harmonic gravity model was implemented using the associated Simulink module in the Aerospace Blockset.

Atmospheric Drag As established earlier, aerodynamic effects significantly perturb the orbit and attitude states of a spacecraft in LEO. The atmospheric density, ρ, is dependent on the satellite position, and is not easily predictable as it varies nonlinearly, by orders of magnitude, with altitude. Numerous atmospheric models have been developed and revised over the years, ranging from the simple exponential to the complex NRLMSISE-00. However, in an effort to minimize the computational cost of the simulations, the lightweight SPeAD-M86 model was incorporated for density estimation. An exhaustive validation of the accuracy of the model is provided by Kedare and Ulrich.[21] The acceleration due to drag is given by

$$\ddot{\vec{r}}_{aero} = -\frac{1}{2} C_D \frac{A}{m} \rho |\vec{v_r}| \vec{v_r} \tag{2a}$$

where,

$$A = \sum_{i=1}^{n} A_n \begin{cases} A_n = 0, & \text{if } \vec{A}_n \cdot \vec{v_r} < 0. \\ A_n = \vec{A}_n \cdot \vec{v_r} & \text{otherwise.} \end{cases} \tag{2b}$$

where m is the spacecraft mass, C_D is the drag coefficient, A is the total projected area perpendicular to $\vec{v_r}$, $\vec{A}_n$ is the area vector for the nth spacecraft panel in the body frame, ρ is the atmospheric density, and $\vec{v_r}$ is the velocity of the spacecraft relative to the atmosphere. The spacecraft drag coefficient, C_D, is a difficult parameter to determine, due to the complex interaction of spacecraft geometry, reflection, molecular content, and spacecraft attitude.[22] Typically, for continuum flows, C_D is in the range of 2 - 4. Vallado and Finkleman[23] provide an overview of research into spacecraft

drag coefficient determination. For the purposes of this study, a C_D of 2.2 was selected, as it corresponds to the free molecular regime as defined by Montenbruck and Gill.[17]

Attitude Dynamics and Kinematics

The rotational motion of an object about its body frame, aligned with the principal axes with the origin at the center of mass, can be defined using Euler's equation for rigid body dynamics and the quaternion kinematic differential equation, presented in Eq. 3 and Eq. 4 respectively.[24] A quaternion attitude representation was selected over the use of Euler Angles to avoid the issues associated with singularities.

$$\dot{\vec{\omega}} = \mathbf{J}^{-1}\left(\vec{T} - \vec{\omega} \times \mathbf{J}\vec{\omega}\right) \tag{3}$$

$$\dot{\mathbf{q}} = \begin{bmatrix} \dot{q_1} \\ \dot{q_2} \\ \dot{q_3} \\ \dot{q_4} \end{bmatrix} = \frac{1}{2} \begin{bmatrix} 0 & \omega_3 & -\omega_2 & \omega_1 \\ -\omega_3 & 0 & \omega_1 & \omega_2 \\ \omega_2 & -\omega_1 & 0 & \omega_3 \\ -\omega_1 & -\omega_2 & -\omega_3 & 0 \end{bmatrix} \begin{bmatrix} q_1 \\ q_2 \\ q_3 \\ q_4 \end{bmatrix} \tag{4}$$

The time rate of change of the attitude states, $\dot{\vec{\omega}}$ and $\dot{\mathbf{q}}$, are multiplexed together to form a state change matrix. The subscripts for each element in the matrices of Eq. (2) represent the row location in the relevant arrays. The torque, $\vec{T}$, is the vector summation of the control torque and environmental torques. The mathematical modeling of the latter shall now be discussed.

Gravity Gradient Torque Any object with finite dimensions orbiting the Earth experiences a differential gravitational force at different radii along its length. This force is akin to the tidal force exerted by the Moon and the Sun on the Earth, the effects of which are visible as daily ocean tides. The differential gravitational force imparts a torque on the satellite about its center of mass*. Equation 5 presents the generalized expression for the gravity gradient torque.[25]

$$\vec{T}_{gg} = \frac{3\mu_{\oplus}}{r_B^3}\left(\frac{-\vec{r}_B}{r_B} \times \mathbf{J}\frac{-\vec{r}_B}{r_B}\right) \tag{5}$$

The transformation of the satellite position from inertial to body coordinates is performed using a direction cosine matrix derived from the quaternion state of the spacecraft. An asymmetric body in a gravitational field will experience a torque aligning the axis of least inertia with the field direction.[26]

Atmospheric Torque The aerodynamic forces acting on a spacecraft do not necessarily act through the center of mass of a spacecraft. This offset results in an aerodynamic torque acting upon the spacecraft, which can be expressed by

$$\vec{T}_{aero} = \sum_{i=1}^{n} \vec{F}_{drag_i} \times \vec{r}_{cp_i} \tag{6}$$

where $\vec{F}_{drag_i}$ is the drag force acting on each spacecraft panel, and $\vec{r}_{cp_i}$ is the center of pressure location of each associated spacecraft panel in the body frame.

---

*C. Hall, Attitude Dynamics and Kinematics, AOE 4140 Lecture Notes, Virginia Tech, 2009 (accessed April 12, 2014), http://www.dept.aoe.vt.edu/ cdhall/courses/aoe4140/

ATTITUDE CONTROLLER

To enable the spacecraft to maneuver into the Orbital Life Extension (OLE) mode, the control system must be capable of reorienting the spacecraft while continually overcoming external environmental torques. The proportional-derivative control law[24] is presented below.

$$\vec{u} = -k\mathbf{J}\tilde{q}_e - c\mathbf{J}\vec{\omega} + \left(\vec{\omega} \times \mathbf{J}\vec{\omega}\right) \tag{7}$$

In Eq. 7, $\vec{u}$ is the commanded control torque, and $\tilde{q}_e$, representing the Eigenaxis of the rotation, consists of the first three elements of the quaternion error. The quaternion error, $\mathbf{q_e}$, is calculated from the current quaternion state, $\mathbf{q}$, and a skew symmetric matrix assembled from the commanded quaternion, $\mathbf{q_c}$.

$$\mathbf{q_e} = \begin{bmatrix} q_{e_1} \\ q_{e_2} \\ q_{e_3} \\ q_{e_4} \end{bmatrix} = \begin{bmatrix} q_{c_4} & q_{c_3} & -q_{c_2} & -q_{c_1} \\ -q_{c_3} & q_{c_4} & q_{c_1} & -q_{c_2} \\ q_{c_2} & -q_{c_1} & q_{c_4} & -q_{c_3} \\ q_{c_1} & q_{c_2} & q_{c_3} & q_{c_4} \end{bmatrix} \begin{bmatrix} q_1 \\ q_2 \\ q_3 \\ q_4 \end{bmatrix} \tag{8}$$

This algorithm presented in Eq. 7 scales the proportional and derivative gain matrices based on the inertia tensor, reducing the overshoot of the controller, and making it globally asymptotically stable. The last term, $\vec{\omega} \times \mathbf{J}\vec{\omega}$, corrects for the gyroscopic moment generated by the inertia tensor during a rotation. The gain coefficient, k, and damping coefficient, c, are functions of the desired system natural frequency and damping ratio defined as follows.

$$k = \omega_n^2 \tag{9a}$$

$$c = 2\omega_n\zeta \tag{9b}$$

In order to verify the ability of a commercially available ACS to perform the OLE maneuver, realistic torque and angular momentum limits had to be enforced upon the control system. MAI-201 Miniature 3-Axis Reaction Wheel system*. The angular momentum of the reaction wheels was calculated through propagation of the reaction wheel state equation, presented below.[27]

$$\dot{\vec{H}}_{RW} = -\vec{u} - \left(\vec{\omega} \times \vec{H}_{RW}\right) \tag{10}$$

where $\vec{\omega}$ denotes the inertial angular velocity of the spacecraft body frame and $\vec{H}_{RW}$ denotes the reaction wheel angular momentum, which saturates at $\pm$10.8E-3 N·m·s based on the specifications of the MAI-201 system. In Eq. 10, $\vec{\omega} \times \vec{H}_{RW}$ is the gyroscopic torque generated by the total reaction wheel momentum. Furthermore, the control torque $\vec{u}$ was limited to $\pm$0.1 mN·m, 16% of the maximum torque of $\pm$0.625 mN·m that the MAI-201 can provide. Operating the reaction wheels at a lower torque could decrease wear and tear of the bearings and contact brushes, and reduce the possibility of equipment failure. The decreased torque also demonstrates the ability of the spacecraft to maneuver with severely degraded reaction wheels.

DRAG SAIL MODELING

Figure 1 illustrates the spacecraft configuration, with deployed drag sails and gravity gradient boom. The drag sails are labeled P1, port ($-\hat{x}$), and S1, starboard ($+\hat{x}$), in accordance with nautical

---

*MAI-201 Miniature 3-Axis Reaction Wheel, CubeSatShop.com, 2014 (accessed Aug. 24, 2014)
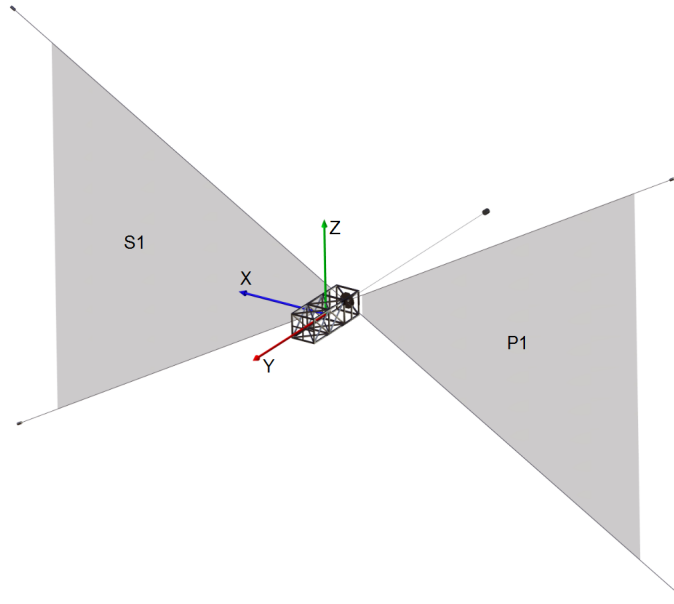
Figure 1. 3U CubeSat Configuration with deployed drag sails and gravity gradient boom

convention. The drag sails, located in the aft section of the CubeSat, are deployed symmetrically about the body y-axis, providing a weathervane stability to the satellite.

From Eqs. (2a), (2b), and 6, accurate modeling of aerodynamic perturbations acting on the CubeSat requires knowledge of the variation in the projected area, as well as information regarding the location of the center of pressure location of each individual panel in the body frame. The 10 faces of the 3U CubeSat body and drag sails were individually defined in the body coordinate frame as area vectors. The center of pressure for each of the panels was similarly specified. Table 1 summarizes the mathematical definition of the satellite geometry.

Table 1. CubeSat Geometry Definition

Panel ID	Label	Area, A (m^2)	Area normal vector, $\hat{A}$	C_P location, $\vec{r}_{cp}$
1	Starboard panel	0.03	$+\hat{x}$	$+(b/2)\hat{x} - (l/3000)\hat{y}$
2	Fore panel	0.01	$+\hat{y}$	$+(l/2)\hat{y}$
3	Zenith panel	0.03	$+\hat{z}$	$-(l/3000)\hat{y} + (h/2)\hat{z}$
4	Port panel	0.03	$-\hat{x}$	$-(b/2)\hat{x} - (l/3000)\hat{y}$
5	Aft panel	0.01	$-\hat{y}$	$-(l/2)\hat{y}$
6	Nadir panel	0.03	$-\hat{z}$	$-(l/3000)\hat{y} - (h/2)\hat{z}$
7	S1 forward face	0.0 - 5.0*	$+\hat{y}$	$+d_x\hat{x} - (l/2)\hat{y}$
8	P1 forward face	0.0 - 5.0*	$+\hat{y}$	$-d_x\hat{x} - (l/2)\hat{y}$
9	S1 aft face	0.0 - 5.0*	$-\hat{y}$	$+d_x\hat{x} - (l/2)\hat{y}$
10	P1 aft face	0.0 - 5.0*	$-\hat{y}$	$-d_x\hat{x} - (l/2)\hat{y}$

*Simulation Variable

The dimensions of the 3U CubeSat are l, b, and h, while d_x represents the C_P location of the drag sails in the $\hat{x}$ direction. These spacecraft parameters are presented later in the Satellite Properties subsection.

SIMULATION RESULTS

Simulink-Matlab was selected for the creation of a simulation environment due to its customizability, modularity, and ease of debugging. The Agilent STK software, though popular for orbit and attitude propagation, does not allow for straightforward implementation of time-variant projected areas. The Smart Nanosatellite Attitude Propagator (SNAP) tool[28] was considered as an option, as it had been extensively verified and utilized in related CubeSat simulations.[14] However, closer examination of the SNAP environment indicated that the effects of atmospheric drag forces on the spacecraft position and velocity were not considered*. Figure 2 visualizes the data flow between each of the simulation environment components described in the previous subsections and illustrates the interdependence of the various modules. The spacecraft dynamics and kinematics block
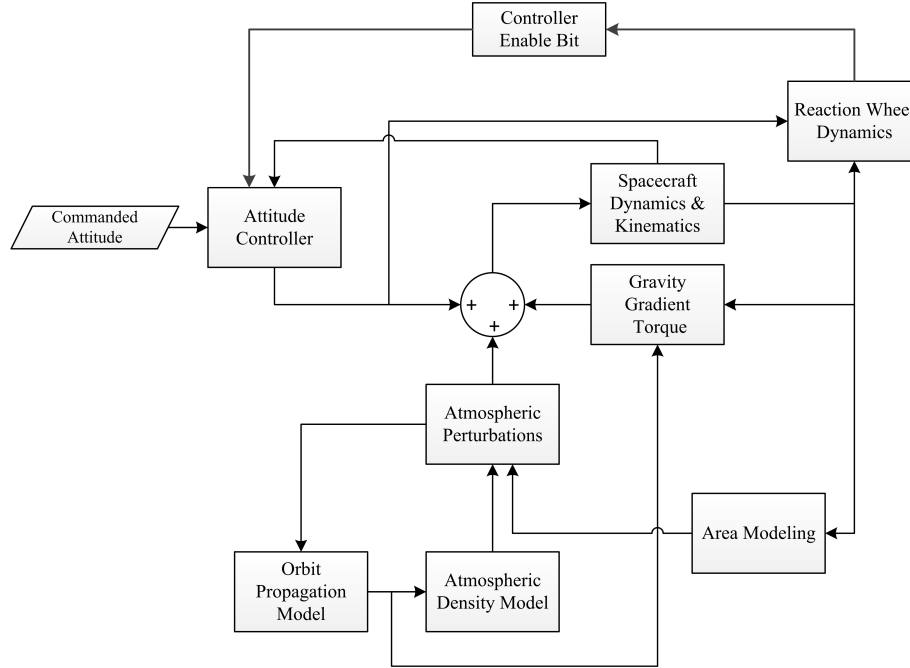

Figure 2. Overview of Simulation Environment Structure

forms the core of the simulation environment, alongside the orbit propagator. The output states from these blocks drive the environmental perturbations which in turn affect the states. The reaction wheel dynamics block models momentum storage, limiting the maximum torque and relaying an interrupt to the controller through an Enable Bit if the maximum momentum capacity is exceeded. All simulations for this study utilized the ode3 (Bogacki-Shampine) integrator for orbit and attitude propagation with 1 second fixed time-steps, and were executed on parallel threads of an Intel®Core™i7 3.9 GHz processor with 16 GB available memory.

---

*Simulation Tools: Smart Nanosatellite Attitude Propagator (SNAP), University of Kentucky Space Systems Laboratory. http://ssl.engineering.uky.edu/simulationtools/snap/

Initial Conditions

The initial classical orbital elements of the satellite with respect to Earth were defined as follows.

$$\begin{bmatrix} a & e & i & \Omega & \omega & \nu \end{bmatrix}_0 = \begin{bmatrix} 6978km & 0.005 & 0.1° & 270° & 90° & 0° \end{bmatrix}$$

These elements correspond to a 565.1 km 634.9 km orbit having a period of 96.7 minutes, with a low inclination of 0.1° to the equatorial plane of the Earth. Such a near-circular orbit is typical for CubeSats, though at a higher altitude compared to prior research. The initial attitude states, $\vec{q}$ and $\vec{\omega}$, of the satellite are presented below.

$$\mathbf{q_0} = \begin{bmatrix} 0 & 0 & 0 & 1 \end{bmatrix}^T \qquad \vec{\omega}_0 = \begin{bmatrix} 0 & 0 & 0 \end{bmatrix} \text{rad·s}^{-1}$$

This corresponds to a satellite with no angular rates aligned with the Earth Centered Inertial (ECI) reference frame.

Satellite Properties

A 3U CubeSat with a mass of 4.0 kilograms in LEO equipped with an on-board 3-axis active attitude control system and deployable drag sails was considered for this study. The satellite dimensions were defined as $l = 0.03$ m, $b = 0.01$ m, and $h = 0.01$ m. The C_P x-location for each drag sail was set as $d_x = 1.0$ m. For rotational stability, $I_{zz} > I_{xx}, I_{yy}$ or $I_{zz} < I_{xx}, I_{yy}$. Such an inertia matrix allows for rotational stability about the axis of maximum or minimum moment of inertia respectively.[25] The satellite inertia tensor $\mathbf{J}$, obtained using the *Mechanical Properties* function in CATIA v5, is now presented for the satellite with drag sails and a single deployable mass along the y-axis.

$$\mathbf{J} = \begin{bmatrix} 0.059 & 0 & 0 \\ 0 & 0.114 & 0 \\ 0 & 0 & 0.126 \end{bmatrix} kg \cdot m^2$$

In addition to the geometric and inertial properties of the satellite, it was necessary to define the controller characteristics. For the purposes of this paper, a damping ratio, $\zeta = 1$ (the critically damped case), and an arbitrary natural frequency $\omega_n = 0.35$, were selected.

Results

Having defined the satellite properties and initial conditions, the simulation results based on the criteria outlined in the Contributions can be presented. Figure 3 presents the variation of ram-pointing error over seven days for four drag sail areas.
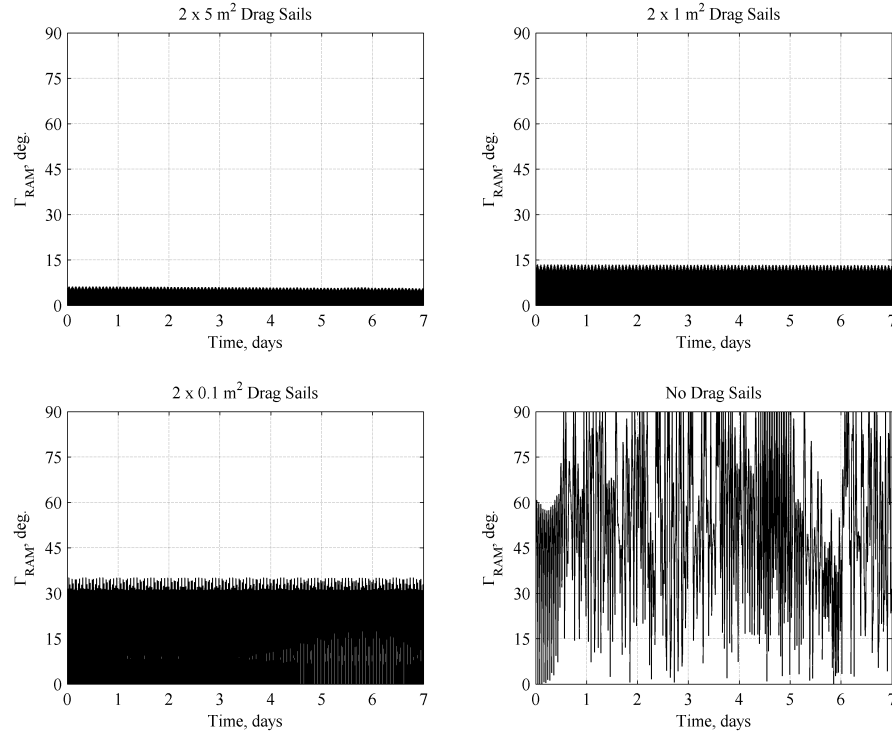

Figure 3. Effect of drag sail area on ram-pointing accuracy

The presence of a pair of drag sails symmetric about the y-axis of the CubeSat prevents the development of uncontrolled oscillations about the ram-pointing orientation. Without drag sails, the spacecraft enters uncontrolled oscillations after approximately 12 hours. The 0.1 m^2 drag sails provide a steady pointing accuracy of $\pm 32°$ over seven days. 1 m^2 drag sails provide an improved pointing accuracy of $\pm 12°$. As in the case of the 0.1 m^2 sails, this pointing accuracy is maintained over seven days. The largest sails considered for this study, with an area of 5 m^2, provide a pointing accuracy of $\pm 6°$. The larger area exerts a greater restoring moment on the spacecraft, allowing for greater pointing accuracy. Having established the effect of the drag sail area on pointing accuracy, it is of interest to examine the oscillation frequency to determine the feasibility of such a system for ram-facing observations. Figure 4 presents the ram-pointing error for the four considered drag sail configurations over the first 240 minutes of the simulation.
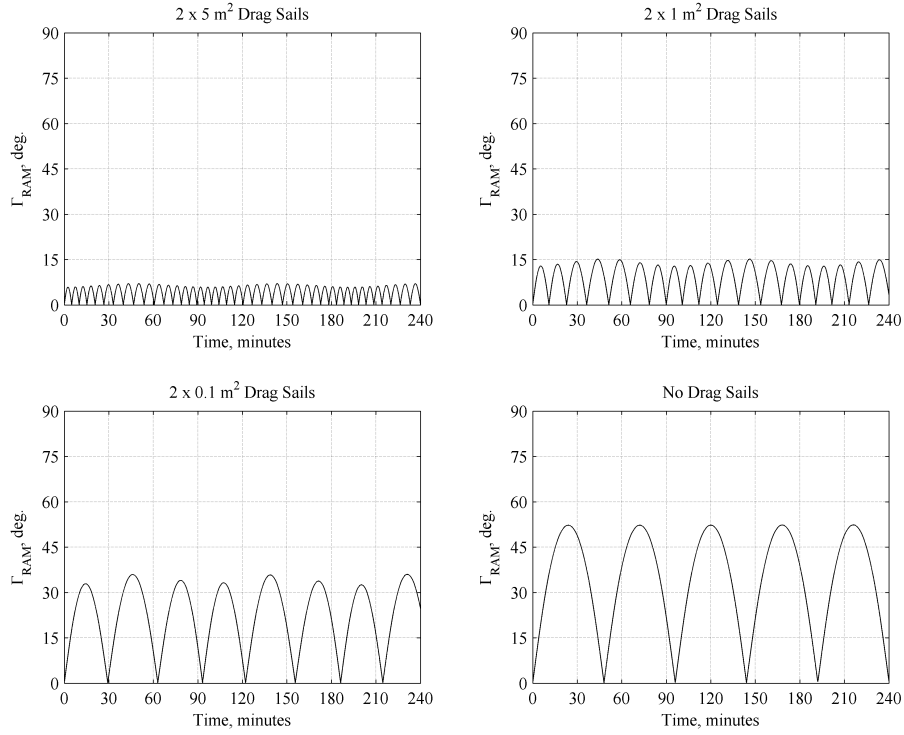
10

Figure 4. Effect of drag sail area on short-term oscillations from ram-direction

Two oscillatory responses are observed for configurations utilizing drag sails - one short term, and one long term. It should be noted that as Γ_{RAM}, the angle between the forward face of the CubeSat and $\vec{v}$, is calculated as an absolute value, one full oscillation is considered to be two consecutive cycles, corresponding to the spacecraft slewing to the left and right of the ram-pointing vector. The short term oscillation are due to the undamped response of the satellite to the environmental torques, while the long term variations, with a period similar to the orbital period, could be the result of spatial variations in the atmospheric density. However, data from the current study is insufficient to conclusively support such a correlation. Interestingly, the control configuration does not appear to exhibit a well-defined long-term oscillation, supporting the possibility that the long-term oscillations are driven by ρ, a function of $\vec{r}$. Table 2 summarizes the effect of drag sail area on the oscillatory characteristics of aerostabilized ram-pointing.

Table 2. Summary of Drag Sail Area Effects on Oscillations

Drag Sail Area (m^2)	Mean Γ_{RAM} (deg.)	Mean Period (min.)	Mean Slew Rate (deg·min^{-1})
5.0	5.7	10.3	1.11
1.0	12	22.4	1.07
0.1	32	60.3	1.06
0.0	52	115	0.90

The results indicate that larger sail areas increase pointing accuracy, and reduce the period of each oscillation. The mean slew rate demonstrates a marginal increase with increasing drag sail area, but remains within $\pm 10\%$ of 1 deg·min^{-1} for the considered sail areas. However, the atmospheric

11

drag which this passive control technique relies upon also affects the orbit of the satellite, and it is therefore impractical to simply increase drag sail areas to achieve greater ram-pointing accuracy. Figure 5 presents the variation in apoapsis and periapsis over seven days for the four sail areas. As
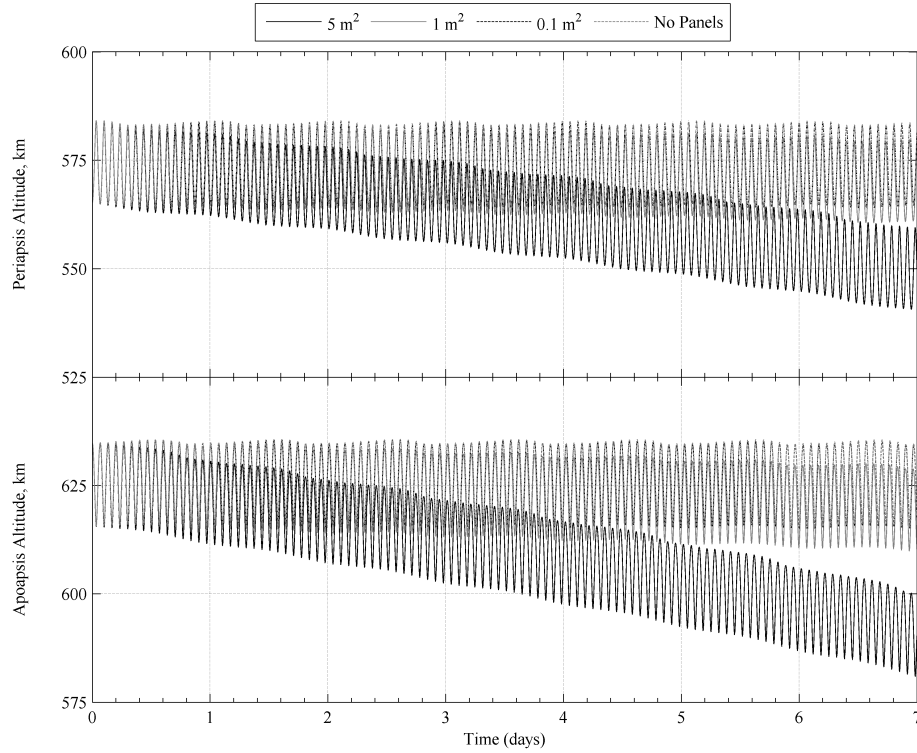

Figure 5. Effect of drag sail area on orbit altitude

expected, the 5 m^2 sails produce the largest drop in orbit altitude with time due to the greater drag force experienced by the satellite. Over seven days, the mean periapsis is reduced by $\approx$25 km, while the mean apoapsis drops by $\approx$35 km. Such sails would be useful if rapid de-orbit of a spacecraft is a requirement. Meanwhile, over seven days, the 1 m^2 sail reduces the mean periapsis and apoapsis by $\approx$5 km and 6 km respectively. In comparison, the 0.1 m^2 sails reduce the mean periapsis and apoapsis by less than 200 m. The information and methodology presented here is sufficient to allow mission planners to perform a preliminary trade study based on the pointing accuracy, oscillation period, and orbital decay rate.

Having examined the effects of the sail areas on satellite pointing accuracy, we now investigate the adaptability of undamped aerostabilization to different inertia tensors. Figure 6 presents the ram-pointing error of four inertia configurations over a period of 240 minutes for a 3U CubeSat equipped with a pair of 5 m^2 drag sails.
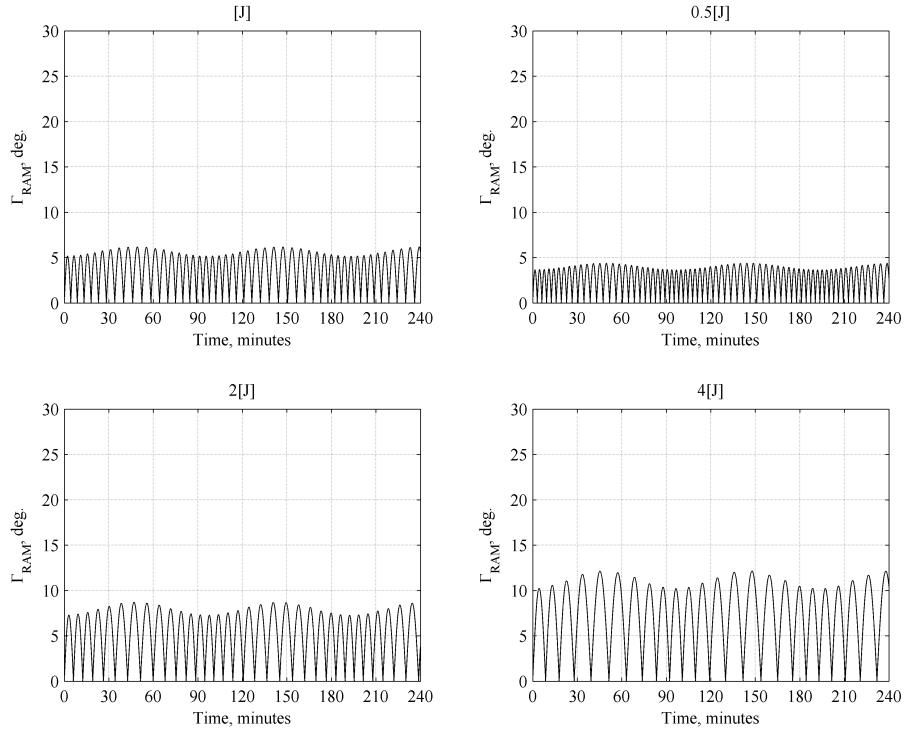
Figure 6. Effect of CubeSat inertia scaling on Oscillation Frequency

Scaling the inertia tensor upwards results in a reduction in pointing accuracy, and an increase in the oscillatory period. Downscaling of **J** produces the opposite effect, i.e., an increase in pointing accuracy, and a decrease in oscillatory period. This agrees with the expected response, as an increased inertia offers greater resistance to external torques. Interestingly, inertia tensor scaling appears to affect the short-term oscillatory response without influencing the long term response. Table 3 summarizes the results.

Table 3. Summary of Inertia Scaling Effects

Inertia Tensor	Mean Γ_{RAM} (deg.)	Mean Period (min.)	Mean Slew Rate (deg·min^{-1})
1.0**J**	5.7	10.3	1.11
0.5**J**	4.04	7.25	1.11
2.0**J**	7.99	14.4	1.11
4.0**J**	11.2	20.1	1.11

Results are for a 3U CubeSat with 5 m^2 drag sails

Figure 7 presents the variation in orbit altitude with the implementation of the Orbit Life Extension (OLE) mode from Day 2 onwards.
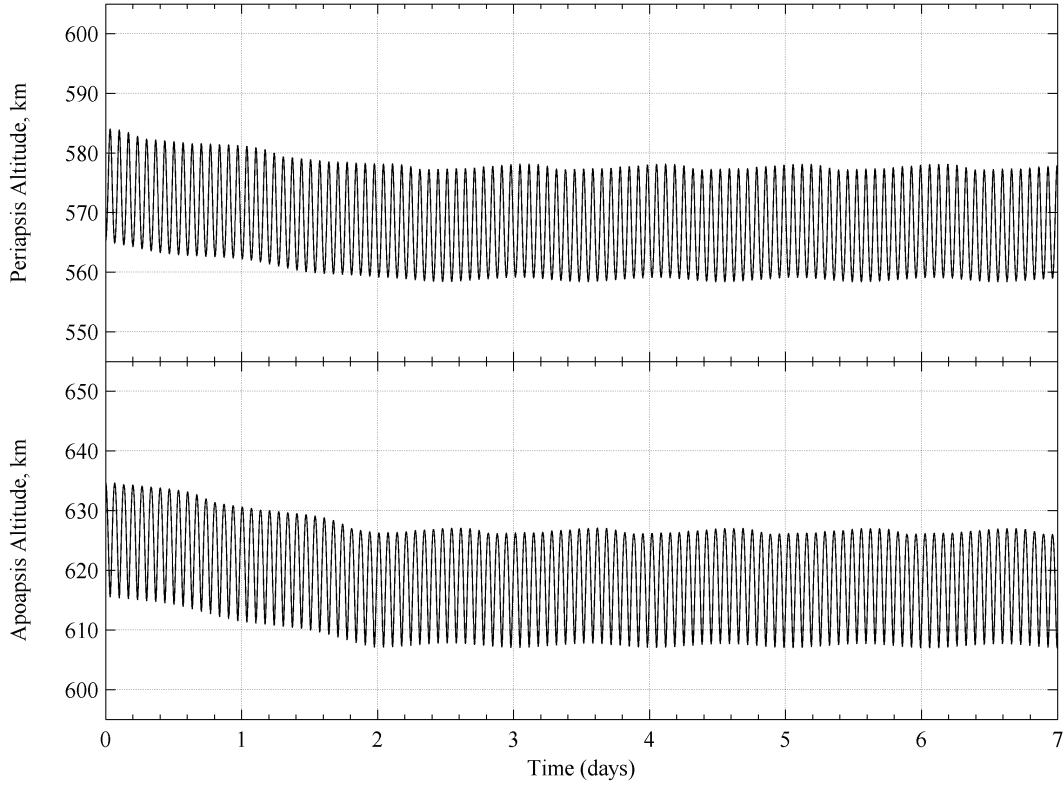
13

Figure 7. Effect of OLE Maneuver on orbit altitude

Over the first two days of the simulation, the mean periapsis and apoapsis drop by 5 km. The satellite maintains a ram-pointing orientation during this time frame, as established in the results presented earlier. Following the execution of the OLE maneuver, the satellite stabilizes in a 570 km x 618 km orbit. The orbital elements for the seven day period presented in Figure 7 is included in Figure A.1 in Appendix A. The results demonstrate that the OLE maneuver can successfully reduce the orbital decay rate of the spacecraft. Figure 8 presents the roll, pitch, and yaw angles for a time window spanning T-120 and T+180 seconds from the activation of the control system. The successfully spacecraft performs an Eigenaxis maneuver from a passive aerostabilized orientation to $[90°\ 10°\ 0°]_{RPY}$ in 135 seconds.
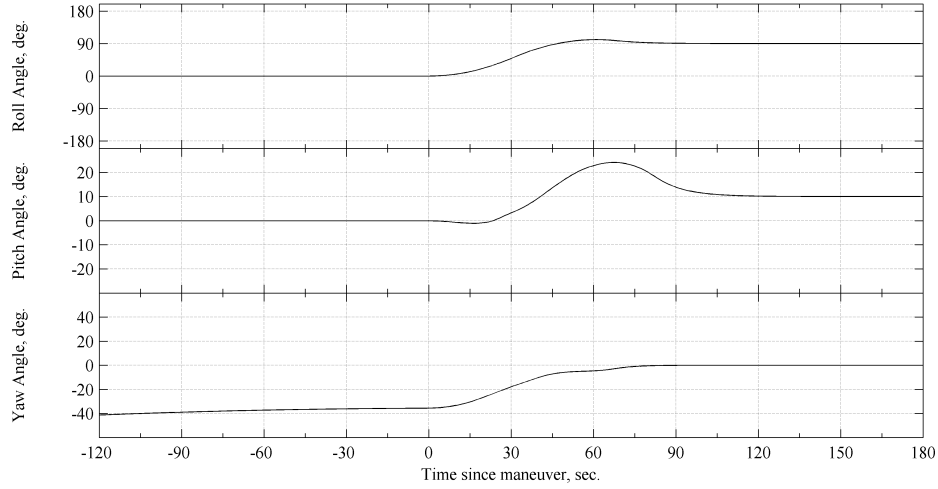
Figure 8. Orbital Life Extension Maneuver

Figure 9 presents the applied torque and angular momentum of the x-, y-, and z-axis reaction wheels of the spacecraft.
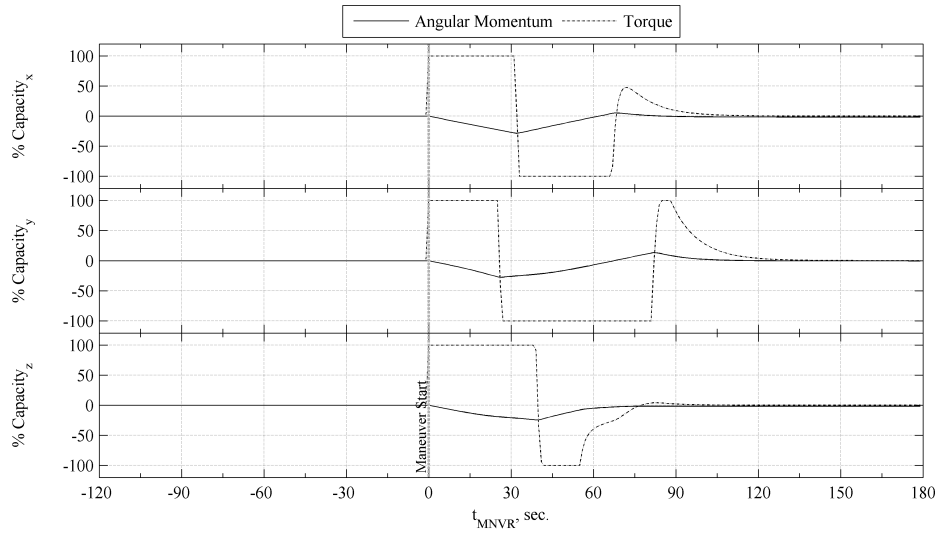

Figure 9. Torque and Angular Momentum Capacity during OLE Maneuver

The allowable torque and angular momentum of the attitude control system remain within the allowable envelope during OLE maneuver. With the torque limited to ± 0.1 mN·m, the controller is capable of overcoming environmental torques, and maneuvers the spacecraft to the commanded attitude. The maximum instantaneous angular momentum capacity utilized during the maneuver was 28.7%, 27.7%, and 24.1% in the x-, y-, and z-axis respectively. Over five days, the spacecraft utilized 12.0%, 0.11%, and 5.74% of the momentum capacity to counteract environmental disturbance torques and maintain a $\begin{bmatrix} 90° & 10° & 0° \end{bmatrix}_{RPY}$ orientation. Figure A.2 in Appendix A provides the angular momentum usage for the entirety of the period.

15

CONCLUSIONS

This work examined the undamped passive attitude characteristics of a 3U CubeSat with deployable drag sails. Two variables - the drag sail area and the satellite inertia tensor **J** - were varied separately to investigate their effects on the ram-pointing accuracy and associated oscillatory response. Larger drag sails demonstrated tighter pointing accuracies, upto a maximum of $5.7°$ from the ram-direction, and decreased oscillation periods, at the cost of faster orbital decay. Upscaling of the inertia tensor decreased the pointing accuracy and increased the oscillation period. However, the reduction in pointing accuracy was minimal, with a $4\times$ inertia scaling corresponding to a pointing accuracy $11.2°$, a decrease of $6°$. In addition to aerostabilization characteristics, an Orbital Life Extension maneuver was analyzed. The simulations indicate that the spacecraft is capable of entering and maintaining a low-drag configuration for five days while utilizing a maximum of 12.0% of available angular momentum capacity to counter environmental disturbances.

The current research opens up a range of potential applications, ranging from high-efficiency passive de-orbit modules to science payloads with rapid de-orbit capability. The sails considered in this study were non-retractable, and once deployed, could not be tacked, manipulated, or altered geometrically. Sails capable of varying their areas with time could be utilized to rapidly desaturate momentum storage devices through intentional application of environmental torques. Furthermore, variable area sails could be utilized as torque augmentation for an active control system, minimizing maneuver times.

Examining the effect of sail quantity and orientation on satellite stability could prove beneficial towards evaluating the potential of origami-inspired drag sails for passive attitude control on Cubesats. Similar deployment and folding techniques were recently demonstrated at NASA's Jet Propulsion Laboratory in Pasadena, CA*.

REFERENCES

[1] A. Toorian, K. Diaz, and S. Lee, "The CubeSat Approach to Space Access," *Aerospace Conference, 2008 IEEE*, Big Sky, MT, March 1-8 2008.

[2] R. Nader, H. Carrion, S. Drouet, M. Uriguen, R. Allu, and G. Naranjo, "NEE-01 PEGASUS: The first Ecuadorian Satellite," *Proceedings of IAC 2011 (62nd International Astronautical Congress)*, Cape Town, South Africa, October 3-7 2011. Paper: IAC-11.B4.1.6.

[3] R. Nader, "Ultra Thin, Deployable, Multi-panel Solar Arrays for 1U CubeSats," *62nd International Astronautical Congress*, Cape Town, South Africa, October 3-7 2011.

[4] Inter-Agency Debris Coordination Committee, *Space Debris Mitigation Guidelines*. in IADC-02-01.

[5] International Organization for Standardization, *Systems - Estimation of Orbit Lifetime*. ISO 27852:2010(E).

[6] D. M. Schrello, "Passive Aerodynamic Attitude Stabilization of Near Earth Satellites," tech. rep., North American Aviation Inc., Columbus, OH, 1961.

[7] J. K. Wall, "The Feasibility of Aerodynamic Attitude Stabilization of a Satellite Vehicle," *American Rocket Society Preprints*, No. 787, 1959.

[8] V. A. Sarychev and M. Y. Ovchinnikov, "Dynamics of a Satellite with a Passive Aerodynamic Attitude Control System," *Cosmic Research*, Vol. 32, No. 6, 1994, pp. 561–575.

[9] R. R. Kumar, D. D. Mazanek, and M. L. Heck, "Parametric and Classical Resonance in Passive Satellite Aerostabilization," *Journal of Spacecraft and Rockets*, Vol. 33, No. 2, 1996, pp. 228–234.

[10] R. R. Kumar, D. D. Mazanek, and M. L. Heck, "Simulation and Shuttle Hitchhiker Validation of Passive Satellite Aerostabilization," *Journal of Spacecraft and Rockets*, Vol. 32, No. 5, 1995, pp. 806–811.

---

*Solar Power, Origami-Style, JPL News Release, Aug. 14 2014, http://www.jpl.nasa.gov/news/news.php?release=2014-277

[11] L. Pacini and D. A. Skillman, "A Passive Aerodynamically Stabilized Satellite for Low Earth Orbit," *Spaceflight Mechanics 1995 : Proceedings of the AAS/ AIAA Spaceflight Mechanics Meeting*, Albequerque, New Mexico, 1995.

[12] S. Rawashdeh, D. Jones, D. Erb, A. Karam, and J. E. Lumpp, Jr., "Aerodynamic Attitude Stabilization for a Ram-Facing CubeSat ," *AAS 32nd Annual Guidance and Control Conference*, Breckenridge, Colorado, 2009.

[13] J. Armstrong, C. Casey, G. Creamer, and G. Dutchover, " Pointing Control for Low Altitude Triple Cubesat Space Darts ," *23rd Annual AIAA/USU Conference on Small Satellites.*, Logan, UT, 2009.

[14] S. A. Rawashdeh and J. E. Lumpp, "CubeSat Aerodynamic Stability at ISS Altitude and Inclination," *26th Annual AIAA/USU Conference on Small Satellites.*, Logan, UT, 2012. SSC12-VIII-6.

[15] G. Bonin, J. Hiemstra, T. Sears, and R. E. Zee, "The CanX-7 Drag Sail Demonstration Mission: Enabling Environmental Stewardship for Nano- and Microsatellites," *27th Annual AIAA/USU Conference on Small Satellites.*, Logan, UT, 2013. SSC13-XI-9.

[16] V. Lappas, S. Pelleggrino, H. Guenat, M. Straubel, H. Steyn, V. Kostopoulos, E. Sarris, O. Takinalp, S. Wokes, A. Bonnema, "DeOrbitSail: De-Orbiting of Satellites using Solar Sails," *2nd International Conference on Space Technology (ICST)*, Athens, Greece, 15-17 Sept. 2011.

[17] O. Montenbruck and E. Gill, *Satellite Orbits: Models, Methods, Applications*, p. 55. Berlin: Springer-Verlag, 2000.

[18] National Aeronautics and Space Administration, *NASA Space Vehicle Design Criteria (GN&C): Spacecraft Aerodynamic Torques*. NASA SP-8058.

[19] F. J. Lerch, C. A. Wagner, D. E. Smith, M. L. Sandson, J. E. Brownd, and J. A. Richardson, "Gravitational Field Models for the Earth (GEM1&2)," Tech. Rep. X55372146, Goddard Space Flight Center, Greenbelt/Maryland, 1972.

[20] N. K. Pavlis, S. A. Holmes, S. C. Kenyon, and J. K. Factor, "The Development and Evaluation of the Earth Gravitational Model 2008 (EGM2008)," *Journal of Geophysical Research: Solid Earth*, Vol. 117, April 2012. DOI: 10.1029/2011 JB008916.

[21] S. S. Kedare and S. Ulrich, "Design and Evaluation of a Semi-Empirical Piece-wise Exponential Atmospheric Density Model for CubeSat Applications," *AIAA Modeling and Simulation Technologies Conference, AIAA Science and Technology Forum 2015*, Kissimmee, FL, 2015. Control ID#: 2024986.

[22] E. M. Gaposchkin, "Calculation of Satellite Drag Coefficients," Tech. Rep. 998, MIT Lincoln Laboratory, MA, 1994.

[23] D. A. Vallado and D. Finkelman, "A Critical Assessment of Satellite Drag and Atmospheric Density Modeling," *Acta Astronautica*, Vol. 92, Feb. - March 2014, pp. 141–165.

[24] B. Wie, *Space Vehicle Dynamics and Control*. Virginia: AIAA Education Series, 1998.

[25] M. Sidi, *Spacecraft Dynamics & Control: A Practical Engineering Approach*. New York: Cambridge University Press, 2002.

[26] M. Sidi, *Spacecraft Dynamics & Control*. New York: Cambridge University Press, 1997.

[27] J.-F. Shi, S. Ulrich, and A. Allen, "Spacecraft Adaptive Attitude Control with Application to Space Station Free-Flyer Robotic Capture," *AIAA Guidance, Navigation, and Control Conference*, Kissimmee, FL, 5-9 January 2015. accepted.

[28] S. A. Rawashdeh and J. E. Lumpp, Jr., "Nano-Satellite Passive Attitude Stabilization Systems Design by Orbital Environment Modeling and Simulation," *Infotech@Aerospace Conference*, Atlanta, GA, 2010. AIAA.
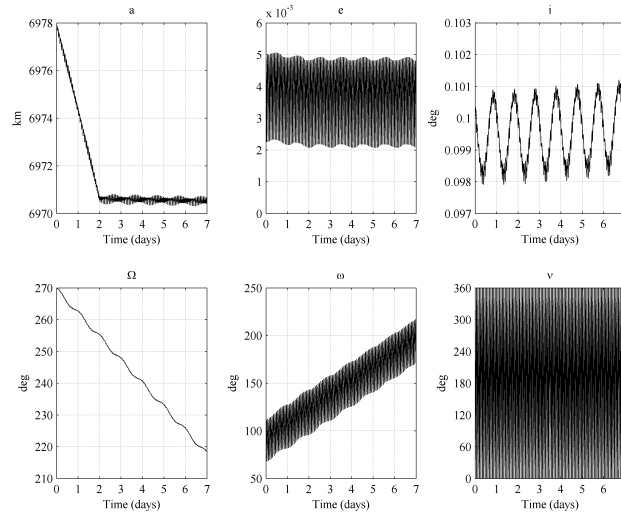
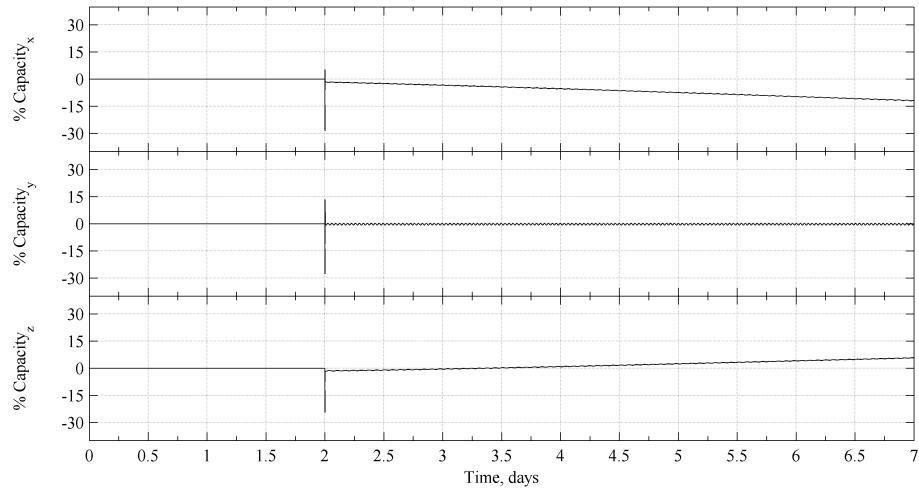# APPENDIX A: ORBITAL LIFE EXTENSION DATA

Figure A.1. Orbital Elements for OLE Mode

Figure A.2. 7 Day Angular Momentum Usage in OLE Mode